Polymer Vol. 37 No. 12, pp. 2403–2414, 1996
Copyright © 1996 Elsevier Science Ltd
Printed in Great Britain. All rights reserved
0032-3861/96/$15.00 + 0.00

Hot-drawing of poly(ethylene terephthalate) under biaxial stress: application of a three-dimensional glass–rubber constitutive model

C. P. Buckley* and D. C. Jones†
Department of Engineering Science, University of Oxford, Parks Road, Oxford OX1 3PJ, UK

and D. P. Jones
ICI Films, PO Box 90, Wilton Centre, Middlesbrough, Cleveland TS90 8JE, UK
(Received 13 June 1995; revised 4 October 1995)

A study was made of the hot-drawing of amorphous poly(ethylene terephthalate) (PET) under biaxial stress in the temperature/strain-rate regime relevant to industrial film drawing. Film specimens were drawn at constant width at temperatures 75–120°C and strain-rates 1–16 s^{-1}, using a specially developed testing machine—the Flexible Biaxial Film Tester. The stress–strain data obtained, together with similar results from uniaxial tests, allowed a recently-proposed three-dimensional constitutive model for amorphous polymers to be tested and applied to PET. It was found that the yield, flow and strain-stiffening observed in drawing could be described well by the model at the lower temperatures. A procedure was devised for systematically fitting data to the model, and produced values of the model parameters which were interpreted in terms of the physical mechanisms of flow and rubber-like strain stiffening. The major inadequacy of the model was that it did not include flow resulting from entanglement slippage, modified in PET by stress-induced crystallization, that intervenes at the upper end of the temperature range. Copyright © 1996 Elsevier Science Ltd.

(Keywords: constitutive model; drawing; biaxial stress; poly(ethylene terephthalate))

INTRODUCTION

There is intense interest in the deformation of poly(ethylene terephthalate) (PET), because of its industrial importance in fibres, film and bottles. The properties of these are usually enhanced in one or two directions, by hot-drawing the polymer during manufacture to introduce molecular orientation. Several authors have studied the hot-drawing process in PET, and the main physical mechanisms involved are widely believed to be known. This suggests it may be possible now to understand and model hot-drawing as it occurs during industrial manufacturing processes. But in fact many difficulties remain. In particular the production of biaxially oriented PET film is characterized by biaxial stresses and rapid rates of strain and temperature change, both of which are difficult to study under controlled conditions in the laboratory. Furthermore, what is needed for engineering purposes is a mathematical model of PET that is three-dimensional and reproduces fully the range of features of constitutive response observed in the glass transition region. This means combining in a single model features that have been studied previously in isolation.

Progress was possible in the present work by exploiting two recent developments. Firstly, a three-dimensional constitutive model has been developed for simulating the behaviour of an amorphous polymer near the glass transition, as described in a recent paper[1]. Secondly, the authors have developed a computer-controlled flexible biaxial film tester (see below), specifically for study of biaxial drawing under the conditions of interest. It has been used to study drawing of films under biaxial stress, to check predictions of the constitutive model and to determine the small number of adjustable constants within it.

It is well known that the hot-drawing of amorphous PET close to the glass transition appears to consist of a flow process constrained by elasticity of a rubber-like network[2]. This is consistent with our analytical model of amorphous polymers near T_g, which is based on the assumption that the free energy (and hence stress) consists of two additive components. One is due to local intra- and intermolecular interactions, and relaxes in shear on an experimental time-scale in the glass transition region (the α relaxation). The other is due to the entropy of conformations of the chain molecules. The first dominates volume change at all temperatures

* To whom correspondence should be addressed
† Present address: Fisons Instruments, 3 Tudor Road, Altrincham, Manchester, WA14 5RZ, UK

and shape change in the glassy region at temperatures below T_g. The second dominates shape change in the rubbery region immediately above T_g. Sufficiently close to T_g the rubber-like stress does not relax on an experimental time-scale and, even though not cross-linked, the polymer is rubbery because topological constraints ('entanglements') act as physical crosslinks. A model that expresses this dual form of behaviour we term here a 'glass/rubber' constitutive model. An early one-dimensional form was proposed by Haward and Thackray[3]. More recently, Boyce and co-workers have generalized the Haward–Thackray model for three-dimensional deformation of polymers in the glassy state, and have found considerable success in applying it to experimental data: see for example Boyce and Arruda[4]. The model used here was introduced as a fully three-dimensional representation of polymer behaviour near T_g, and differs in certain respects as discussed elsewhere[1].

Such a model will be most directly applicable to a non-crystallizable non-crosslinked polymer of very high molecular weight, at temperatures where the rate of conformational relaxation by entanglement slippage is negligible. Its application to conventional film and fibre grade PET needs some justification, as (i) the number average molecular length lies within an order of magnitude of the length of chain between entanglements, and therefore entanglement slippage is expected to be relatively rapid and the 'plateau region' in time and temperature where the polymer shows rubber-like response will be particularly narrow; (ii) PET is well known to crystallize during hot-drawing. Nevertheless, there is substantial evidence for a temperature region close to T_g where these effects do not perturb significantly the constitutive response of PET, and its behaviour can be described without reference to entanglement slippage or crystallization directly. Ward and co-workers, in particular, have shown that PET drawn uniaxially at temperatures just above the glass transition behaves as a rubbery network polymer[5–7], and recently extended the evidence to biaxial drawing[8].

Development of crystallinity is apparent as a measurable rise in density beginning at a stretch (draw ratio) of about 2 or higher and the emergence of a wide angle X-ray diffraction pattern[9]. It is not yet certain how developing crystallinity affects the rheology of PET. Earlier work by Buckley and Salem, however, showed that when drawn PET fibres with low levels of crystallinity were further crystallized, the dominant mechanical effect was to lengthen the relaxation time for an additional viscoelastic relaxation process observed above the glass transition, that they christened the α' relaxation[10]. They suggested that the α' process in PET, even when partially crystallized, corresponds to the slippage of entanglements (reptation) normally seen in polymer melts. On this basis, crystallization is expected simply to reduce the contribution of entanglement slip to the constitutive response, and hence improve agreement with the representation of PET as a rubbery network polymer. Indeed it provides the best explanation for why conventional fibre and film grades of PET conform so well to a description in terms of a rubbery network, considering how low are their usual molecular weights. It is on this premise that the glass/rubber constitutive model has been applied to PET in the present work.

The purpose of this paper is firstly to demonstrate that the three-dimensional constitutive model provides a good description of rapid hot drawing of amorphous PET under biaxial stress in certain circumstances, and to define those where it does not. Secondly, it is to obtain values for the few unknown parameters of the model for PET, by fitting of experimental data.

EXPERIMENTS

Flexible biaxial film tester

Experiments were carried out with the purpose-built testing machine developed by the authors for biaxial tensile testing of polymer films, under conditions comparable to those encountered in the manufacture of high performance, biaxially oriented films. Because it offers an unusual degree of flexibility in the design of experiments, we have termed it a Flexible Biaxial Film Tester (FBFT). Details were given elsewhere[11]. It will suffice here to recall just the salient features of the FBFT.

For biaxial stress experiments, each specimen took the form of a 70 mm square of film, held around its perimeter by 24 grips, each of which was a pneumatically operated piston/anvil combination. On each of the two perpendicular axes, grips on opposite edges of the specimen were moved apart by a reverse thread leadscrew driven by a brushless d.c. servo-motor, controlled by computer software. In addition, a stepper motor controlled by the same software drove a rotary heat-valve mixing hot and cold air, providing a supply of variable-temperature air blowing on one surface of the specimen, in a manner similar to that described for fibres by Buckley and Sikorski[12]. The reverse face was thermally insulated.

During experiments, a Biodata 'Microlink' data-logging system captured signals from force transducers on central grips on each axis and also from thermocouples measuring the air-jet temperature. From the force measurement, specimen thickness and the portion (11 mm) of specimen width associated with the central grip, the stress was determined. Specimen temperature was obtained from the air temperature, making use of a prior calibration when air temperature had been measured simultaneously with specimen temperature (determined with an embedded thermocouple). Experiments were then carried out fully automatically, under computer control, by a program which set up the motion profiles for the three motors, initiated the test and then obtained the measured signals of force and temperature from the data-logger. Uniaxial tests were also carried out with the FBFT, but the square specimen was replaced by a 10 mm × 70 mm strip of film, with a dummy square specimen mounted immediately behind it, to provide the same thermal environment as in a biaxial stress test.

Material

The polymer used in this work was ICI PET homopolymer with number average molecular weight $\bar{M}_n = 19\,000$ and diethylene glycol content of only 2.7 mol%. Isotropic amorphous film was prepared by melt extrusion through a slit die onto a chilled roller held at 10°C and then wound up to produce a film with

nominal thickness 250 μm. The measured density was 1339 kgm^{-3} and wide angle X-ray scattering showed no evidence for diffraction, indicating the absence of crystallinity. In-plane birefringence was found to be only 1.4×10^{-4}, confirming that in-plane molecular orientation in the as-extruded film was negligible. Although, for consistency, in the experiments described here specimens were always mounted in the FBFT with the machine direction of extrusion parallel to machine axis 1, no significant difference was found in results when directions were reversed.

Experimental procedure and results

The particular biaxial stress experiments reported here consisted of drawing film specimens in one direction while constrained at constant width in the transverse direction. For comparison, further experiments consisted of conventional uniaxial drawing. All the drawing experiments were carried out at high nominal strain-rates between 1 and 16 s^{-1}, in the range typical of industrial film drawing.

The following procedure was adopted. First, the film specimen was marked with a square ink grid. It was mounted in the grips of the FBFT, and soaked in blown air at the test temperature for 2 min. The drawing test was then initiated, and the specimen extended to a draw-ratio of 4 at a constant nominal strain-rate, either uniaxially or at constant width. On completion of the test the heat-valve was closed rapidly, quenching the specimen to room temperature before its removal from the test rig. The final measured deformation of the grid, at the specimen centre and along its centre-line, was used to calibrate clamp separation in terms of strain, assuming a constant ratio between them throughout the test. In all experiments reported here, strains were found to be approximately uniform within the specimen, with no formation of a neck. Actual values of strain quoted here refer to the central region of the specimen where the stress was measured.

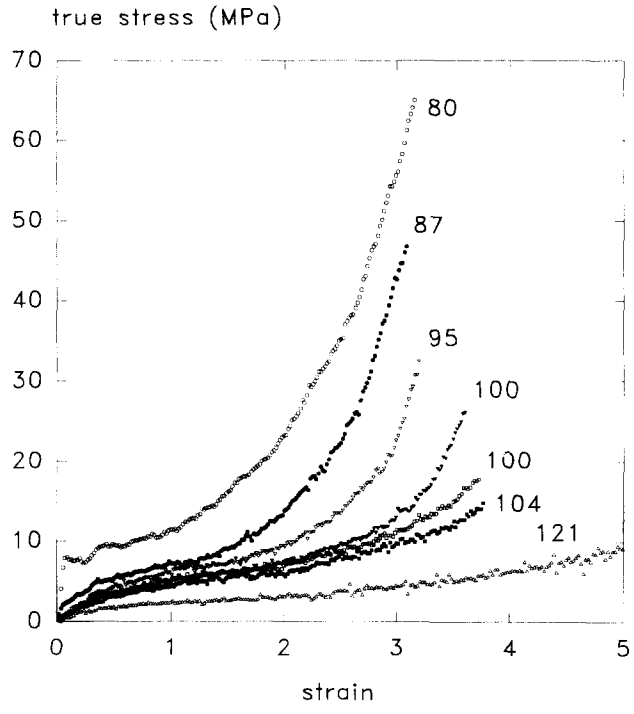

Figure 1 Example plots of true stress (in the direction of drawing) *versus* nominal strain for constant-width drawing of amorphous PET, at a nominal extension-rate of 1/s and various temperatures (°C) as shown

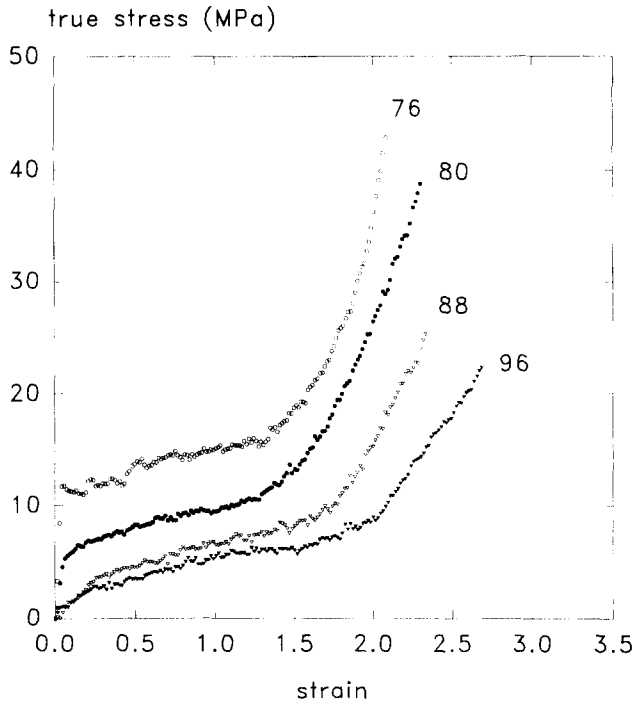

Figure 2 Example plots of true stress *versus* nominal strain for uniaxial drawing of amorphous PET film at a nominal extension-rate of 1/s and various temperatures (°C) as shown

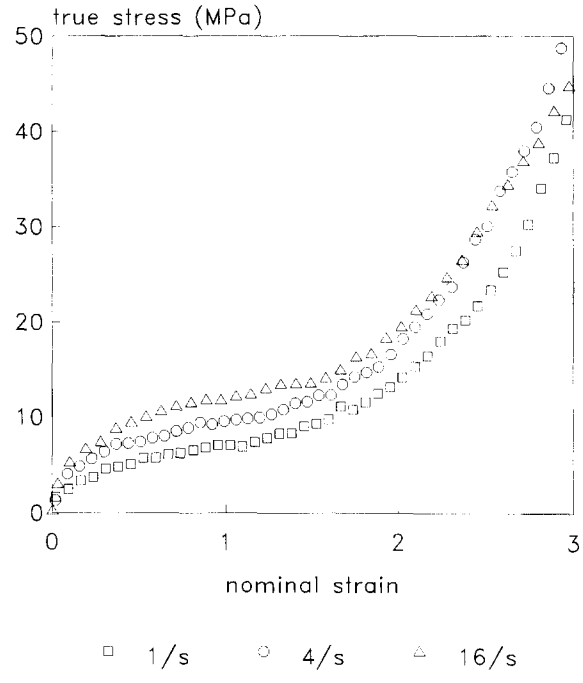

Figure 3 Example plots of true stress *versus* nominal strain for constant-width drawing of PET at three extension-rates shown and temperature 87°C

Some results for constant-width drawing at a constant nominal extension-rate of 1/s and various temperatures are shown as graphs of true stress σ_1 *versus* nominal

strain in *Figure 1*. *Figure 2* shows similar data for uniaxial drawing, for comparison. Further results, showing the effects of varying the extension-rate on constant-width drawing, are shown in *Figure 3*. In each case the true stress was calculated from nominal stress data obtained from the data-logger, assuming deformation was at constant volume. In *Figure 3*, the cross-over of curves for 4/s and 16/s is believed to reflect adiabatic heating at the higher extension rate.

At the strain-rates used in these tests, isothermal conditions cannot be assumed *a priori*. An upper limit on the extent of adiabatic heating was estimated by measuring the coefficient of heat transfer between the specimen and the blown air, and then computing the temperature rise of the specimen from a heat balance applied to it, given the work input from the measured applied stress and extension-rate: the extreme assumption was made that none of the strain energy was stored as inter-atomic potential energy, as explained by Adams[13]. The greatest calculated temperature rise was *ca.* 10 K, reached at the ends of those tests with the highest stresses and extension-rates. Usually, however, it was much less than this. For a nominal strain-rate of 1/s, the maximum equilibrium temperature rise was calculated to be approx. 5 K per MPa of nominal drawing stress at the initial specimen thickness, but reducing during the test as the specimen became thinner. In practice such a figure was never reached, as the time constant for achieving steady-state heat transfer was over 9 s and tests were considerably shorter than this.

The pattern of results was typical of the drawing behaviour of PET at temperatures just above the glass transition, as seen before by many authors for uniaxial drawing, and recently for constant-width drawing at slower rates by Gordon *et al.*[8]. In the cases of both uniaxial and constant width drawing an apparent yield region was clear at strains in the region of 0.1–0.5. This was followed by pronounced strain-stiffening, which has been attributed frequently in the literature to chain-straightening as occurs in elastic deformation of a rubber-like network. Notable features of the results were that rubber-like strain-stiffening was deferred to higher strains and the yield region became less localized in strain with an increase in temperature, as can be seen in *Figures 1* and *2*.

APPLICATION OF CONSTITUTIVE MODEL

Summary of the model

A detailed description of the glass–rubber constitutive model was given elsewhere[1]. An outline will suffice here. It rests on the hypothesis that the change in free energy at any instant can be expressed as the sum of two terms. One is due to perturbation of inter- and intramolecular inter-atom potentials, and may be loosely termed 'bond-stretching'. The other is due to perturbation of chain statistics as expressed by the conformational entropy. The bond-stretching free energy does not account for the full macroscopic stretch, as there is an additional viscous flow due to breakage and reformation of intermolecular bonds, made possible by the molecular segmental motion which commences near the glass transition. Conversely, conformational entropy *is* assumed uniquely determined by the total macroscopic stretch, as the entangled polymer chains behave as a rubber-like network with respect to the statistics of chain conformation.

Consider an irrotational deformation expressed by the stretch tensor $\mathbf{\Lambda}$, whose eigenvalues are the principal stretches λ_i ($i = 1, 2, 3$). It follows from above that the Cauchy (true) stress tensor $\mathbf{\Sigma}$, principal values σ_i ($i = 1, 2, 3$), can be expressed as the sum of a *bond-stretching stress* $\mathbf{\Sigma}^b$ and a *conformational stress* $\mathbf{\Sigma}^c$, and that for the ith principal direction a stress balance may be written:

$$s_i^b + K^b \sum_{j=1}^{3} \epsilon_j + \sigma_{m0}^b + \sigma_i^c - \sigma_i = 0 \qquad (1)$$

where s_i^b are principal components of the deviatoric part of $\mathbf{\Sigma}^b$, K^b is the contribution to bulk modulus arising from bond-stretching and ϵ_j are principal natural strains $\ln \lambda_i$. The additional constant stress σ_{m0}^b represents the in-built, zero-strain, hydrostatic perturbation of inter-atomic potentials, required to balance the zero-strain entropic compression. Splitting the deviatoric strain-rate into an elastic part associated with bond stretching and a viscous part associated with intermolecular bond breakage and re-formation, it may be expressed:

$$\frac{ds_i^b}{dt} + \frac{s_i^b}{\tau} = 2G^b \frac{de_i}{dt} \qquad (2)$$

in which e_i are deviatoric parts of the natural strains, and the time constant $\tau = \mu/2G^b$, where G^b is the contribution to shear modulus arising from bond-stretching and μ is a non-Newtonian viscosity function.

The viscous flow process is assumed to follow the generic Eyring formulation for an activated rate process[14], allowing the possibility that the activation step includes a momentary dilation. Applying the Eyring theory then leads to the following expression for the viscosity in terms of the invariants of $\mathbf{\Sigma}^b$: octahedral shear stress τ_{oct}^b and mean stress σ_m^b (it is convenient to express the latter as the perturbation from its zero-strain value: $\Delta\sigma_m^b = \sigma_m^b - \sigma_{m0}^b$)

$$\mu = \mu_0 \left(\frac{\tau_{oct}^b V_s}{2RT}\right) \frac{\exp\left(\dfrac{-\Delta\sigma_m^b V_p}{RT}\right)}{\sinh\left(\dfrac{\tau_{oct}^b V_s}{2RT}\right)} \qquad (3)$$

where μ_0 is the viscosity in the low stress (Newtonian) limit and in turn may be expressed in terms of temperature T, fictive temperature T_f (characterizing the structure of the amorphous polymer) and its value μ_0^* at some reference state (T^*, T_f^*):

$$\mu_0 = \mu_0^* \exp\left(\frac{C}{T_f - T_\infty} - \frac{C}{T_f^* - T_\infty} + \frac{\Delta H_0}{RT} - \frac{\Delta H_0}{RT^*}\right) \qquad (4)$$

In equation (3), V_s and V_p are the shear and pressure activation volumes respectively and R the universal gas constant. In equation (4), C and T_∞ characterize the temperature-dependence of free volume, while ΔH_0 is the activation enthalpy.

The model is completed by an expression for the conformational stress in terms of the conformational free energy function A^c

$$\sigma_i^c = \frac{1}{\det \mathbf{\Lambda}} \frac{\partial A^c}{\partial \ln \lambda_i} \qquad (5)$$

Many suggestions for the form of the function A^c have been made in the literature of rubber elasticity. In the

present work, the Edwards-Vilgis[15] expression was employed. For an entangled and crosslinked polymer in the limit of no crosslinks, it yields:

$$A^c = \frac{N_e k_B T}{2}\left(\frac{(1+\eta)(1-\alpha^2)}{(1-\alpha^2\sum\lambda_i^2)}\sum\frac{\lambda_i^2}{1+\eta\lambda_i^2} + \sum\ln(1+\eta\lambda_i^2) + \ln\left(1-\alpha^2\sum\lambda_i^2\right)\right) \quad (6)$$

(all summations are over $i = 1$–3), where N_e is the number of entanglements per unit volume, η is a measure of the delocalization of entanglement points as they are envisaged to have some freedom to displace along the molecule, and α is a measure of the inextensibility of the network defined in terms of the distance a between entanglements and the length l of a freely orienting segment: $\alpha = l/a$. If $\eta = \alpha = 0$ the Gaussian case is recovered from equation (6).

Application to experimental data

Results from the drawing experiments described above were analysed, firstly to test the validity of the model for PET, and secondly to determine a set of the material properties required for describing PET in terms of the model. Methods were devised for obtaining these from measurements of yield, drawing and small strain (linear) viscoelasticity:

(i) properties obtained from uniaxial and biaxial yield and flow: μ_0, V_s, V_p.
(ii) properties obtained from strain-stiffening during drawing: N_e, α, η.
(iii) properties obtained from the linear viscoelastic response: ΔH_0, C, T_∞, G^b, K^b.

The first two sets of properties were obtained from data obtained in the present study. The remainder were obtained by reference to the literature for PET. The steps employed are given below.

First it is convenient to cast the equations in a form suitable for comparing with data for yield under general biaxial stress. In terms of the model, yield corresponds to flow at constant Σ^b. Let the ratio of in-plane natural strain-rates be θ:

$$\frac{1}{\lambda_2}\frac{d\lambda_2}{dt} = \frac{\theta}{\lambda_1}\frac{d\lambda_1}{dt} \quad (7)$$

and let the ratio of strain-induced in-plane bond-stretching stresses be ξ:

$$\Delta\sigma_2^b = \xi\Delta\sigma_1^b \quad (8)$$

At yield and beyond, it follows from equation (2) and the good approximation $\Delta\sigma_3^b = 0$ that

$$\xi = \frac{2\theta+1}{\theta+2} \quad (9)$$

Under these conditions the natural strain-rate along axis 1 becomes, from equations (2) and (3)

$$\frac{1}{\lambda_1}\frac{d\lambda_1}{dt} = \frac{\sqrt{2}(2-\xi)}{\sqrt{1-\xi+\xi^2}}\left(\frac{RT}{\mu_0 V_s}\right)\exp\left[\frac{\Delta\sigma_1^b(1+\xi)V_p}{3RT}\right] \times \sinh\left[\frac{\Delta\sigma_1^b\sqrt{1-\xi+\xi^2}V_s}{3\sqrt{2}RT}\right] \quad (10)$$

When the argument of the sinh term is large compared to unity, equation (10) may be rearranged to give an explicit expression for the bond-stretching contribution to the flow stress on axis 1:

$$\frac{\Delta\sigma_1^b}{T} = \frac{6R}{2(1+\xi)V_p + \sqrt{2}\sqrt{1-\xi+\xi^2}V_s} \times \left(\ln\left[\frac{1}{\lambda_1}\frac{d\lambda_1}{dt}\right] + \ln\left[\frac{\sqrt{2}\sqrt{1-\xi+\xi^2}\mu_0 V_s}{(2-\xi)RT}\right]\right) \quad (11)$$

The equations were checked against experimental data and fitted to them in the following sequence of steps.

Step 1: the 'Eyring plot'

The constant-width drawing experiments described above provided measurements of stresses on axes 1 and 2, at given values of temperature (T), extension-rate and stretch on axis 1 ($\dot{\lambda}_1$ and λ_1), and biaxiality ratio (θ). In the following discussion only σ_1 from constant width experiments is employed: i.e. $\sigma_1(T, \dot{\lambda}, \lambda)$ with $\theta = 0$, where λ refers to the stretch on axis 1. From results of experiments at a range of extension-rates and at 87°C,

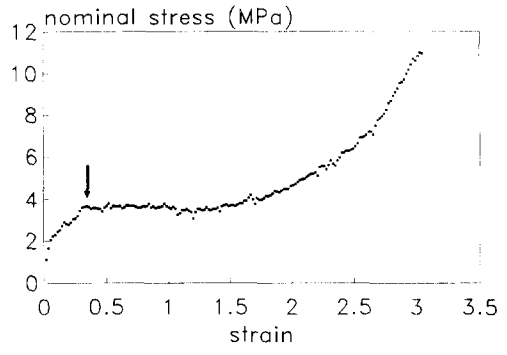

Figure 4 Typical output data from the FBFT testing machine during constant-width drawing of PET at an extension-rate of 1/s and temperature 87°C: nominal stress *versus* nominal strain. The arrow marks the start of the yield 'plateau' in nominal stress, taken to be the 'yield point' for the purposes of this work

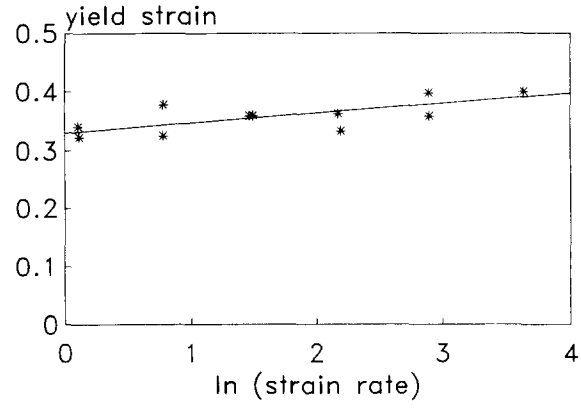

Figure 5 Nominal strain at yield, for constant-width drawing experiments on PET at various nominal strain-rates. Yield was taken as the start of the plateau in nominal stress, as illustrated by the arrow in *Figure 4*

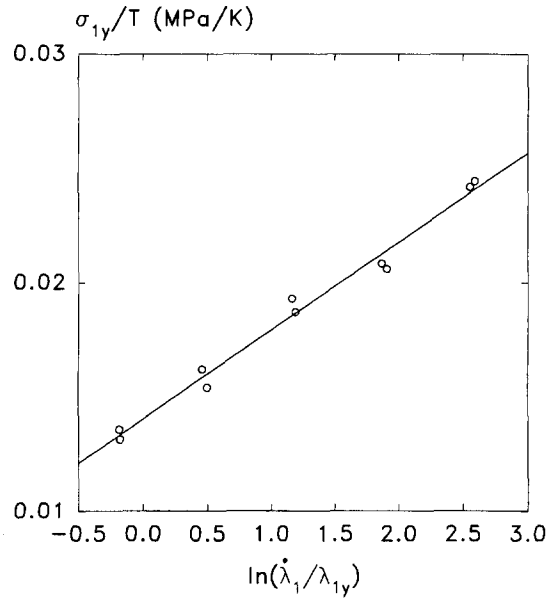

Figure 6 Eyring plot for constant-width drawing of PET at 87°C: true stress at yield (in the direction of drawing) expressed as σ_y/T plotted *versus* the natural strain-rate at yield $\dot{\lambda}/\lambda_y$

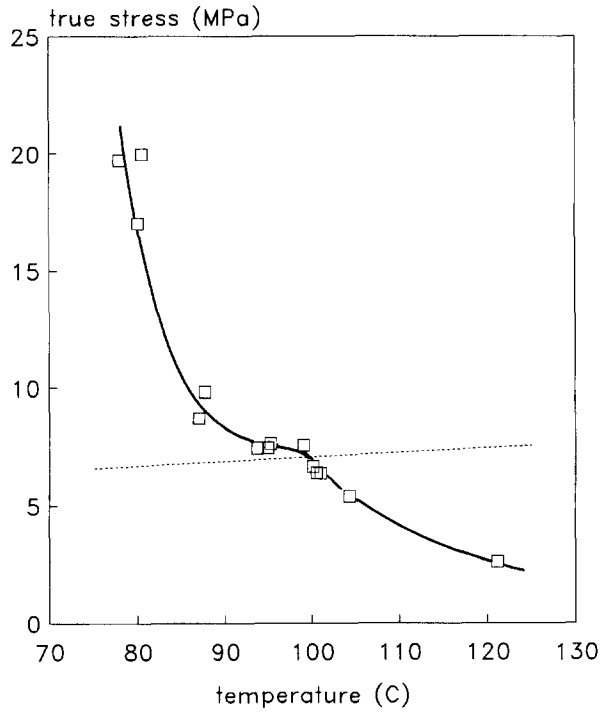

Figure 7 Isometric plot of true stress (in the direction of drawing) at $\lambda = 2.3$ as a function of temperature for constant-width drawing of PET. A small rubbery plateau is discernible. The dotted line shows the rubbery asymptote in the absence of entanglement slippage

yield points were identified as the start point of the yield plateau in nominal stress on axis 1, at a stretch λ_y. An example set of data is reproduced in *Figure 4*, as nominal stress *versus* nominal strain. The point denoted 'yield' for this experiment is marked by an arrow. The nominal strain at yield, determined in this manner, was found to be approx. 0.3, varying only slightly with extension-rate over the range investigated as can be seen in *Figure 5*.

The corresponding true stresses at yield σ_{1y} were used to construct the 'Eyring plot' of σ_{1y}/T *versus* $\ln(\dot{\lambda}/\lambda_y)$ shown in *Figure 6*. The plot showed good evidence for linearity:

$$\frac{\sigma_{1y}}{T} = m \ln\left(\frac{\dot{\lambda}_1}{\lambda_{1y}}\right) + c \qquad (12)$$

where m and c were constants. This is to be expected from equation (11), since the conformational contribution to stress will be constant at constant strain and any variation is due to σ_1^b. A least squares fit to the open points in *Figure 6* gave $m = 3.87 \pm 0.17 \times 10^{-3}$ MPa K^{-1}; $c = 1.41 \pm 0.03 \times 10^{-2}$ MPa K^{-1}. Note that this procedure ignored slight differences in temperature at yield at the various extension-rates due to different degrees of adiabatic heating. However, the computed difference in temperature between the highest and lowest extension rates was only 0.3 K.

Step 2: identification of the rubber-like plateau

To separate out and quantify the conformational component of stress in the PET of the present study is difficult, because of the close proximity of the onset of entanglement slippage to the glass transition region. This may be seen from isometric plots of stress *versus* temperature, as shown in *Figure 7* for CW drawing to a stretch $\lambda = \lambda^* = 2.3$. Nevertheless there is clear evidence for a short plateau region 90–100°C, where the stresses s_i^b have relaxed but conformational relaxation by entanglement slippage has not commenced. At the plateau PET is deforming apparently as a rubber. The dotted line represents the estimated rubber-like stress at this stretch, assumed proportional to absolute temperature.

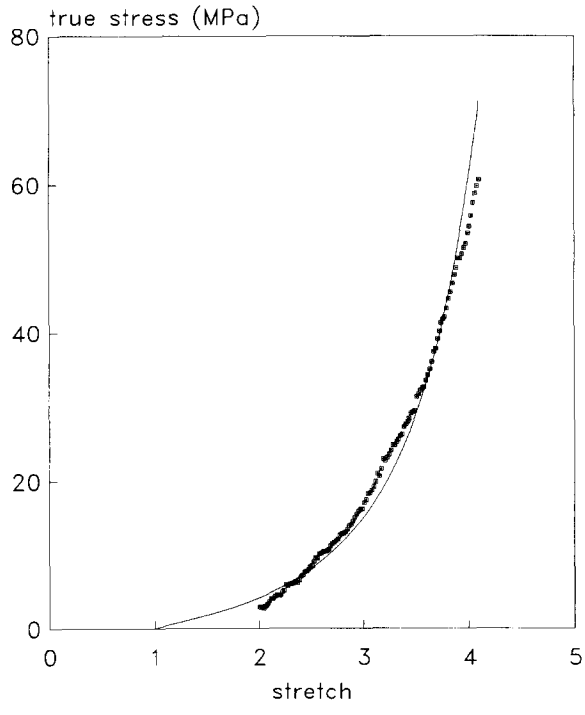

Figure 8 Data points: estimated true stress *versus* stretch for constant-width stretching of the PET rubbery network, extracted from measured data as described in the text. (——) Stress as calculated from the theory of Edwards and Vilgis[15] fitted to the data, assuming incompressibility

Step 3: calculation of rubber-like stress–strain curve

The rubber-like stress–strain curve (where bond-stretching stresses are fully relaxed) was obtained over a wider range of strain using measured stress–strain data for constant width drawing at 80°C and an extension-rate of 1/s, the low temperature being chosen to minimize the contribution of entanglement slippage at high strains. The method adopted was to subtract out from the total measured true stress in direction 1 the contribution from bond-stretching. The latter was deduced from the rubber-like stress already estimated at $\lambda = 2.3$, and corrected for the varying rate of natural strain as predicted by equation (11). Thus the rubber-like stress σ_1^R at a stretch λ was calculated from

$$\sigma_1^R(\lambda) = \sigma_1(\lambda) - \left[\sigma_1(\lambda^*) - \sigma_1^R(\lambda^*) - m\ln\left(\frac{\lambda}{\lambda^*}\right)\right] \quad (13)$$

where $\lambda^* = 2.3$. The resulting estimated rubber-like stress–strain curve for 80°C is shown in *Figure 8*. (This procedure ignored adiabatic heating by up to 7 K, which is believed to be occurring at this temperature over the strain range for which the rubber-like stress–strain curve was determined: the maximum error in $\sigma_1^R(\lambda)$ from this source is 4 MPa, at the highest strain.)

Step 4: fitting of rubber-like response to the Edwards–Vilgis theory

These data were then least-squares fitted to the rubber-like stress–strain curve for constant width stretching, as predicted by the Edwards–Vilgis (E–V) free energy function—equation (6), together with the assumption of incompressibility, to obtain best values for the three parameters appearing in this function: $N_e = 1.67 \times 10^{26}\,m^{-3}$, $\alpha = 0.180$, $\eta = 0$. The resulting calculated stress is included as the full line in *Figure 8*. The fit to the data can be seen to be reasonable. There is, however, a small but systematic discrepancy, which more recent work in our laboratory suggests is caused by the onset of entanglement slippage even at 80°C[16].

Step 5: calculation of activation volumes and limiting (low stress) viscosity

With the aid of the E–V free energy parameters, the rubber-like contribution to yield stresses plotted in *Figure 6* was calculated for the mean stretch at yield ($\lambda_y = 1.355$), and subtracted from c to give a modified value c' applying to σ_1^b alone. Comparing equations (11) and (12), it can be seen that c' corresponds to the constant term on the right-hand side of equation (11), while m corresponds to the term multiplying $\ln(\dot{\lambda}_1/\dot{\lambda}_{1y})$. These together with a similar treatment of the measured uniaxial yield stress for $T = 87$°C and $\dot{\lambda} = 1$/s were used to compute the three parameters of the Eyring flow model: $V_s = 7.23 \times 10^{-3}\,m^3\,mol^{-1}$, $V_p = 1.35 \times 10^{-3}\,m^3\,mol^{-1}$, $\mu_0 = 6.77$ MPas.

Step 6: temperature-dependence of linear viscoelastic response

Literature data for linear viscoelastic creep and stress relaxation of PET, in the temperature region below the dilatometric glass transition (*ca.* 67°C according to Kolb and Izard[17]), were employed to obtain the activation enthalpy ΔH_0, via the reported time–temperature shift factors $\ln a_T = \ln(\mu_0/\mu_0^*)$ and equation (4) with $T_f = T_f^*$. From the range of data available, those of Murayama *et al.*[18] and Vallat *et al.*[19] were chosen as most reliably relating to stable specimens (T_f = constant), and gave a mean value of $123\,kJ\,mol^{-1}$ (assumed independent of orientation and crystallinity), but with a large degree of uncertainty (values ranged from 84 to $187\,kJ\,mol^{-1}$. With ΔH_0 estimated, time–temperature shift factors measured by Ward[20] for creep of unoriented semicrystalline PET above the glass transition (where $T_f = T$) were fitted to equation (4), to obtain the constants C and T_∞. The results were: $C = 435$ K; $T_\infty = 322$ K.

Step 7: elastic constants of glassy PET

Finally, values were assigned to the elastic constants of glassy amorphous PET. The early torsion pendulum study of PET by Illers and Breuer[21] provided a value of G^b from the unrelaxed shear modulus G^U in the temperature region just below T_g: $G^b \approx G^U = 600$ MPa. A reliable value for the unrelaxed bulk modulus K^U of amorphous PET in the glassy state could not be found in the literature. Instead, the corresponding Poisson's ratio was assigned a value typical of amorphous polymers below the glass transition: $\nu^U = 0.35$, and hence the required bulk modulus was obtained: $K^b \approx K^U = 1.8$ GPa.

DISCUSSION

The present results allow a critical assessment to be made of the validity of the constitutive model for PET, and also provide a set of material parameters with physical significance. We consider each aspect of the model in turn.

Testing the model

At its heart is the assumption that stress is separable into two contributions relaxing on different time/temperature scales, so that they can be identified and characterized separately. Such an approach is suggested by the behaviour of uncrosslinked polymers in the linear viscoelastic region. Provided the molecular weight is sufficient for significant molecular entanglement, they exhibit two major relaxations on distinct time/temperature scales, corresponding to the onset of backbone chain segmental motion and slippage of entanglements respectively. At an intermediate time or temperature known as the "plateau region" the polymer, even though uncrosslinked, behaves as a rubber–elastic network. In the present work we have tested whether the same approach can be applied throughout the range of strain by examining isometric plots of stress *versus* temperature for constant extension-rate tests, as shown for example in *Figure 7*. As already noted, a small but distinct plateau in stress was indeed observed, allowing us to quantify separately the parameters governing the two contributions to the stress response.

The major assumption concerning relaxation of the bond-stretching stress is that the flow can be represented as the non-Newtonian viscous flow of an isotropic material. It is then expressible as the second term in equation (2), with all viscoelastic nonlinearity embodied in the stress dependence of a generalized viscosity function μ. The assumption leads directly to equation

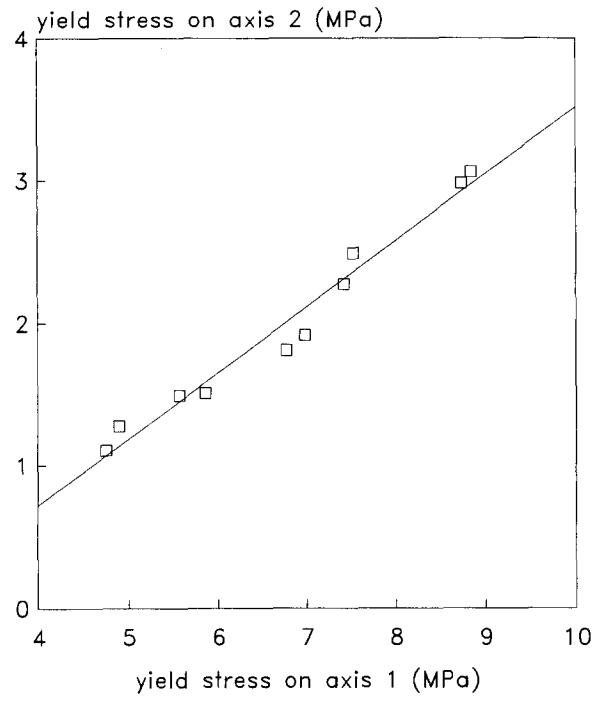

Figure 9 Transverse stress at yield plotted *versus* axial stress at yield, for constant-width drawing of PET at various extension-rates at 87°C. The regression line through the points has a gradient of 0.47, to be compared with the value of 0.5 predicted by the flow rule assumed in this work [equation (9)]

(9), giving the ratio of post-yield, in-plane, bond-stretching stresses during biaxial drawing. In particular, for the case of constant width drawing $\theta = 0$, hence $\xi = 1/2$. The constant width drawing experiments of the present study allowed this to be tested, by plotting the stress measured at yield on axis 2 (transverse direction) *versus* the yield stress on axis 1 for experiments carried out at various extension rates, as shown in *Figure 9*. Since yield strains were almost independent of strain-rate (*Figure 5*), the conformational contributions to stress at yield were constant, and we expect a straight line relation with gradient 1/2. The data are in reasonable agreement giving the first order regression line shown, with correlation coefficient 0.984, and gradient 0.47, supporting the form of flow model used here.

The second assumption concerning the flow process is that it can be described in terms of Eyring kinetics, and this is supported by the apparent linearity of the plot shown in *Figure 6*. The values of activation volumes obtained suggest that the activation event is a co-operative process involving large numbers of atoms: V_s and V_p correspond to 12 and 2.2 nm^3 respectively, equivalent to 50 and 9 monomer units respectively.

Significance of the model parameters

The values obtained for the shear and pressure activation volumes are equivalent, when combined, to apparent activation volumes of 7.2 and 4.2 nm^3 for uniaxial tension and compression respectively. These are consistent, for example, with the value of 4.0 nm^3 given by the uniaxial compressive data for PET at room temperature obtained by Argon and Bessonov[22]. They are also of the same order as obtained by many authors who have applied a simplified one-dimensional Eyring analysis to the uniaxial tension or compressive plastic deformation of polymers: for example, Haward and Thackray quote values in the range 3–28 nm^3 for a range of polymers[3]. It is important to recognize that these cannot be equated to the physical volumes of material involved—each activation volume represents a product of a volume and a strain increment [for example, see equation (14) in Buckley and Jones[1]]. In fact, recent atomic-level simulations of plasticity in glassy polymers show that plastic strains associated with the activation event may be only 1–2%[23,24]. Assuming a similar value applies to PET, the physical volume involved is as high as about 530 nm^3, corresponding to spheres of radius 5 nm.

A further important assumption of the present model is that a single non-Newtonian flow process accounts for all inelasticity in the polymer response in the time/temperature region considered here. Thus, from equation (2), it is the same process that gives rise to linear viscoelasticity at low stresses as causes yield and flow at high stresses. Such remarkable simplicity in the polymer behaviour can only be suggested tentatively at present, and merits further study, but a range of circumstantial evidence supports it as discussed by Buckley and Jones[1]. The present work provides a further item of evidence. As mentioned above, the process of fitting constant width and uniaxial yield stress data to equation (11) gave, in addition to the two activation volumes, a value for the low stress limit of the viscosity: μ_0. From this may be obtained the linear viscoelastic shear relaxation time $\tau_0 = \mu_0/2G^b$. Since $1/2\pi\tau_0$ gives the frequency of the G'' loss peak (in Hz) in a linear viscoelastic, dynamic mechanical experiment, it may be compared with measurements reported in the literature for the glass transition in amorphous PET. This is done in *Figure 10*,

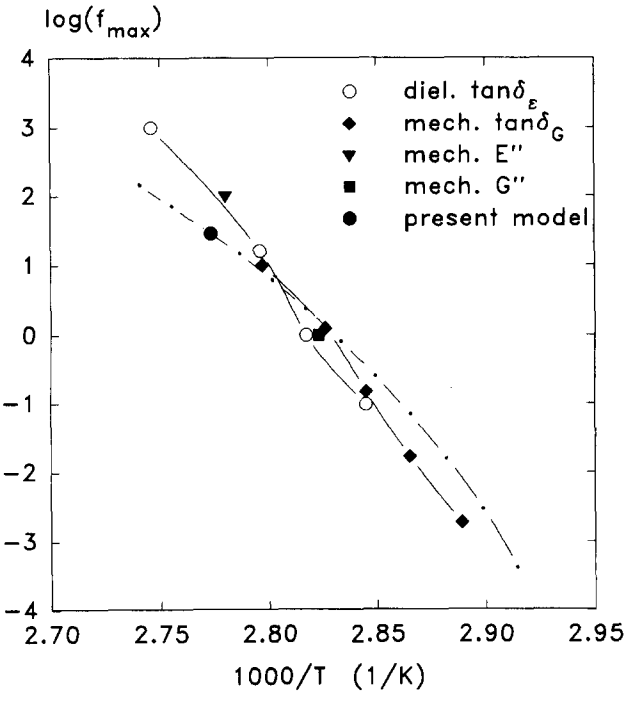

Figure 10 Frequency of maximum loss at the glass transition of amorphous PET, as calculated for G'' from the present model using yield data (●), and as obtained from mechanical and dielectric measurements in the linear viscoelastic region, as quoted by Illers and Breuer[21]

where the filled circle shows the value calculated *from yield data* in the present work at the temperature where it was obtained (87°C), the chain curve shows its temperature-dependence given by equation (4), and the remaining points are from a variety of *linear viscoelastic* measurements quoted by Illers and Breuer[21]. Remarkably, there is only a small discrepancy between the calculated point obtained from yield and the measured linear viscoelastic data.

Use of the E–V free energy function to account for the conformational component of stress receives some support from the degree of fit shown in *Figure 8* between the rubber-like stress–strain curve of PET and that calculated for an E–V rubber. Further work is needed to determine whether the small but systematic discrepancy indicates inadequacy in the E–V free energy function itself or alternatively that the rubber-like curve for PET has not been isolated fully by the method used here. Nevertheless the parameters obtained from the fit give insight into the nature of the entanglement network in PET.

The best fit value of η was found to be zero. In terms of the E–V theory this indicates that entanglements in PET behave as crosslinks with no freedom to slide. An explanation might be the bulk of the terephthalate residue in the polymer backbone, restricting relative displacement between a PET chain and its neighbours. The result is important, as it justifies the widespread practice of treating PET in this temperature range as a crosslinked rubber. It is interesting to note however that, when comparing their shrinkage stress values from uniaxially drawn fibres with the E–V theory, Long and Ward found evidence for two regimes of draw ratio, with $\eta \approx 0$ at low strains ($\lambda < 1.8$) but with η values of 0.26–0.62 at higher strains. No such evidence was found in the present data, where rubber-like stress–strain data were always fitted best with $\eta = 0$: the explanation may lie in the perturbing effect of strain-induced crystallization on the shrinkage stress data.

N_e corresponds to the number density of network strands between entanglements, and is related to the molecular weight between entanglements M_e thus:

$$N_e = \frac{\rho N_A}{M_e}\left(1 - \frac{2M_e}{\overline{M_n}}\right) \qquad (14)$$

where the second term is the Flory correction term for dangling ends. Inserting $\overline{M_n}$ for the PET of the present work yields $M_e = 3200$: there are 16.7 monomers between entanglements (viz. 100.2 backbone bonds, since there are 6 of these per monomer). Further information on the network comes from the number of freely orienting segments per network strand, given by $n = 1/\alpha^2 = 30.9$ if the network strand is assumed to be a random walk. Combining these two numbers yields a value for the number of backbone bonds per freely orienting segment = 100.2/30.9 = 3.24; but see below.

It is interesting to compare these values with those proposed by previous authors who have considered PET as a rubbery polymer in the region above T_g. A means used by Ward and co-workers to estimate the rubber-like stress–strain relation of PET has been the measurement of the peak shrinkage stress, on heating the drawn polymer at constant length[6,7]. Comparing results with the simplified Gaussian theory of rubber elasticity, the entanglement density was found to be $1.8 \times 10^{26}\,m^{-3}$ by Pinnock and Ward[5], $1.89 \times 10^{26}\,m^{-3}$ by Rietsch and Ward[6], and $2.63 \times 10^{26}\,m^{-3}$ by Long and Ward[7]. Caution is needed, as there is no exact correspondence between the peak shrinkage stress and the rubber–elastic component of the drawing stress. Nevertheless, these values do indicate a consistency with the present determination of N_e to within approx. 7%. When the same parameter has been deduced in the past from stress–strain data directly, without sufficient precautions taken to isolate the rubber-like component of stress, values obtained for N_e show wider scatter: Rietsch and War in uniaxial drawing found $2.4–9 \times 10^{26}\,m^{-3}$, while Gordon *et al.*[8] found $1.5–2.32 \times 10^{26}\,m^{-3}$ from uniaxial and constant width drawing. There remains, however, an unresolved inconsistency. Measurements of the small strain plateau shear modulus of PET by Wu[25] and by Le Bourvellec (cited by Lorentz and Tassin[26]) indicated the much higher entanglement densities of 5.56×10^{26} and $6.72 \times 10^{26}\,m^{-3}$ respectively. The origin of this discrepancy is not yet known. However, one might speculate that at small strains the free energy contains, in addition to the conformational entropy, a contribution from energy–elastic interactions (perhaps by π-bonding) between chains even in shear above the glass transition.

There is also conflicting evidence on the flexibility of the PET molecule. As noted above, the fitting of the E–V model to the rubber-like stress–strain curve obtained in this work indicates a flexible chain with only 3.2 backbone bonds per freely-orienting segment. This is not supported by values deduced from the characteristic ratio C_∞ of PET. Flory[27] calculated $C_\infty = 4.15$ using the rotational isomeric states model of PET, and this lies within the range of measured values obtained from solution viscosities. It indicates a figure of 9.3 for the number of backbone bonds per freely-orienting segment. On the other hand, Ward and co-workers, combining the measured stress–optical coefficient of PET in the supposedly rubbery state with the calculated difference in principal polarizabilities of the PET monomer and assuming the Gaussian theory, have consistently obtained values covering the range 15.2–19.8 backbone bonds per freely-orienting segment[5,6,8].

With specific features of the model checked against experiment as described above, and values for the parameters determined, it is possible to examine its overall performance in a wider range of situations. Since the equations of the model form a system of simultaneous nonlinear differential equations, a numerical solution is required in general. In the present work algorithms were developed for solving the equations of the model numerically, under uniaxial and general plane stress conditions, and implemented in computer programs. Inputs were the time-sequences of λ_1, or of λ_1 and λ_2 in uniaxial and biaxial cases respectively. Outputs in the uniaxial case were $\sigma_1(t)$ and $\lambda_2(t) = \lambda_3(t)$, and in the biaxial case were $\sigma_1(t)$, $\sigma_2(t)$ and $\lambda_3(t)$. In both cases, the procedure employed was to approximate the differential equations by ordinary equations in the changes in the outputs through a time-step, and then to solve the resulting simultaneous nonlinear equations by the Newton–Raphson method. To ensure stability and accuracy, whilst also simulating large strains, it was

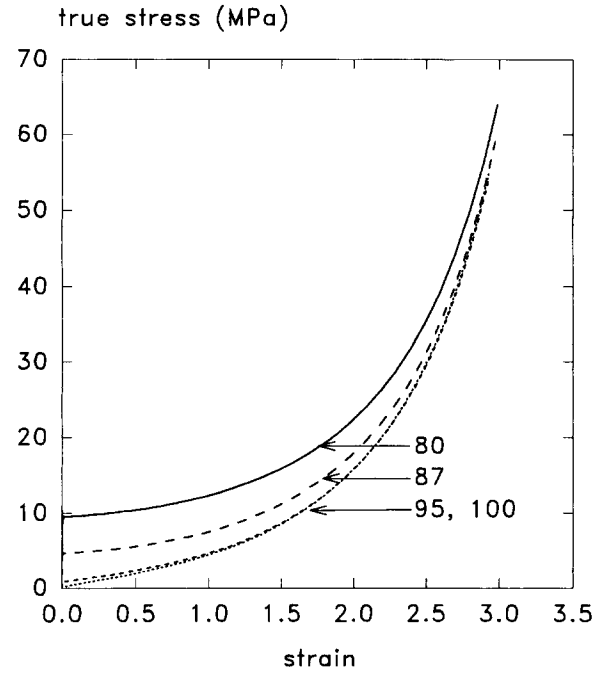

Figure 11 Stress–strain curves for drawing of amorphous PET at constant width, as computed with the constitutive model proposed in the text for an extension-rate of 1/s and various temperatures (°C). The corresponding experimental data are given in *Figure 1*

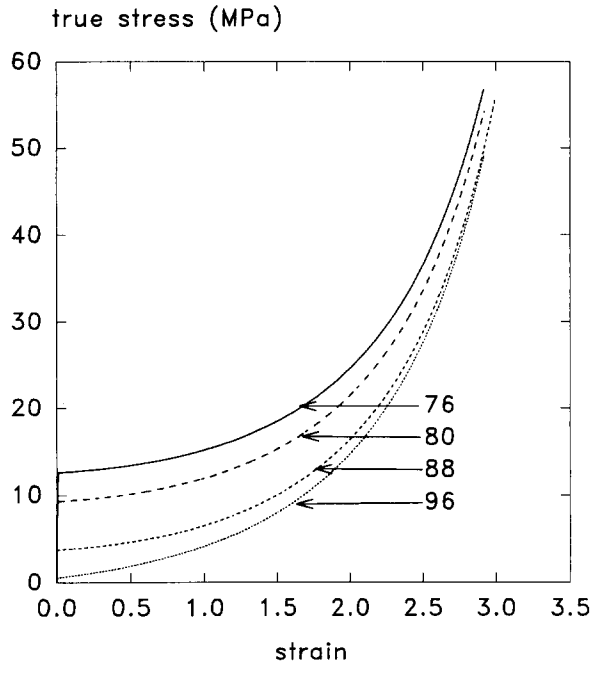

Figure 12 As *Figure 11*, but for uniaxial drawing. The corresponding experimental data are given in *Figure 2*

found necessary to use a varying time step size. A practical problem with the form of constitutive model used here is the high degree of non-linearity associated with exponential stress-dependencies of the Eyring viscosity [equation (3)]. This means that a conventional finite difference approximation of the differential equations sometimes required inconveniently small time steps in the region of yield, if accuracy and numerical stability were to be preserved. This problem was overcome, and a more robust solution obtained, by integrating the differential equation analytically through the time-step, as described in the Appendix.

Results from simulations of a variety of uniaxial straining sequences at large and small strain were discussed in the previous paper[1], where it was shown that the model is successful in simulating a wide variety of features in the responses of amorphous polymers.

With the computer programs, simulations were carried out of isothermal, constant extension-rate, uniaxial and constant-width drawing of PET at temperatures within the region of interest. Since this lies above the glass transition, the structure of amorphous PET as specified by fictive temperature T_f was assumed to be constant during straining, with $T_f = T$. Typical computed stress–strain curves for constant width drawing and uniaxial drawing respectively are shown in *Figures 11* and *12*. They are to be compared with the experimental stress–strain curves plotted in *Figures 1* and *2* respectively. The simulation results clearly share the major features of experimental results. In both cases there is a 'yield' region where apparently plastic deformation commences, followed by extensive flow and pronounced strain-stiffening. Of course, because all flow in the simulated polymer is constrained by conformational elasticity, the plasticity is only apparent: upon release, the simulated polymer film eventually fully recovers (shrinks back to its original dimensions).

The major discrepancies between measured and simulated stress–strain curves lie in the details of their shapes at small and large strains. At small strains, the simulated 'yield' region is clearly confined to a much narrower range of strain than observed experimentally, as noted before[1]. Such behaviour is a well-known feature of constitutive models of an Eyring or similar type and is clearly visible in the work of Haward and Thackray[3] and the more recent papers of Boyce *et al.*[4]. In terms of the present model, it is a consequence of assuming there to be only one activation free energy barrier, and hence a single relaxation time τ. In practice, in the linear viscoelastic range it is well known that a spectrum of relaxation times is required for fitting data, implying the existence of a spectrum of free energy barriers. Buckley and Babaiikochekseraii[28] extended the present model to include such a spectrum, and showed that it also led to a broadening of the yield region as required to obtain agreement with experiment. A similar approach was adopted in more recent work on the modelling of yield in the glassy region by Hasan and Boyce[29].

The discrepancy at large strains is the clear tendency for simulated stress–strain curves at different temperatures to converge with increasing strain, not seen in experimental data. It is due to a combination of factors. Firstly there is a reduction in contribution from the temperature-dependent flow stress, as the natural strain-rate falls with increasing strain. Secondly the entropic conformational stresses, that dominate at large strains, increase with increase in temperature. The reason convergence is not seen in experimental data (*Figures 1* and *2*) is believed to be the onset of entanglement slippage, which the present model ignores, and which relaxes the conformational contribution to stress. This entanglement slippage increases progressively with both temperature and time in the constant extension-rate tests. It may be incorporated quantitatively by expressing

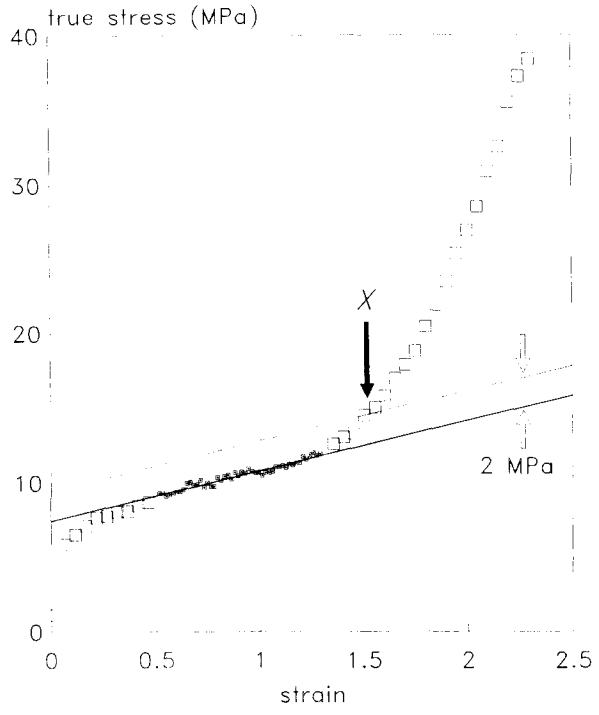

Figure 13 Illustration of the empirical procedure used to determine the strain corresponding to 2 MPa strain-stiffening (see text for explanation). The data here are for uniaxial drawing of amorphous PET at extension-rate 1/s and temperature 80°C

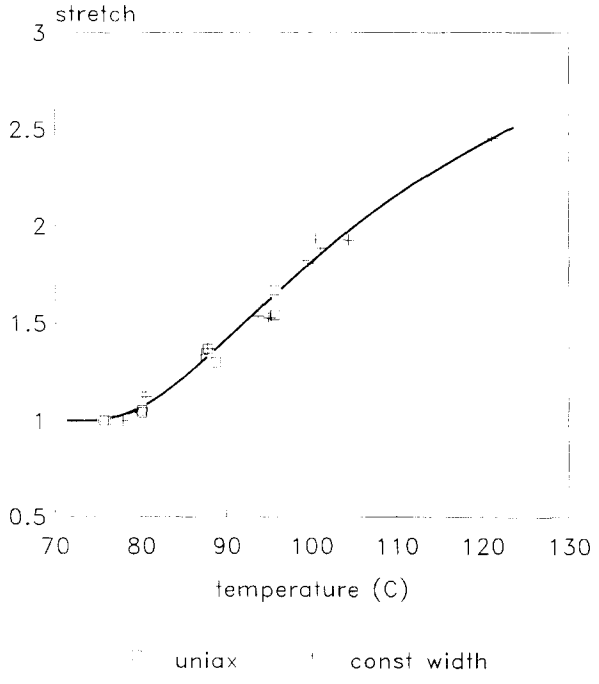

Figure 14 The stretch λ^S due to slippage of entanglements, as determined at 2 MPa strain-stiffening from stress–strain data for uniaxial or constant width drawing following the procedure of *Figure 13*

the total stretch in terms of a 'network stretch' tensor Λ^N, relative to the unloaded state, and an irreversible 'slippage stretch' Λ^S:

$$\Lambda = \Lambda^N \Lambda^S$$

For uniaxial or constant width drawing, in the direction of drawing for example $\lambda = \lambda^N \lambda^S$.

An empirical measure of the contribution of λ^S, at constant λ^N, was obtained from stress–strain curves as shown in *Figure 13*. On each of the measured constant extension-rate stress–strain curves, the inflection region between yield and strain-stiffening was identified and used as a baseline, in order to determine the point X on the curve corresponding to 2 MPa strain-stiffening (chosen arbitrarily). In *Figure 13*, the small filled points were chosen for linear regression to obtain the baseline (thick line shown), and the construction line (thin line shown) was used to determine the point of 2 MPa strain-stiffening. With the stretch λ^X at the lowest temperatures (78 and 80°C) assumed equal to λ^N (i.e. entanglement slippage assumed to be absent), values at higher temperatures gave measures of the stretch associated with entanglement slippage from $\lambda^S = \lambda^X/\lambda^N$. Results are shown in *Figure 14* for both uniaxial and constant width cases. Although they refer specifically to a strain-stiffening of 2 MPa, the same trend is observed if some other degree of strain-stiffening is used. The stretch associated with entanglement slippage increases systematically with increase in temperature, and to within the sensitivity of its estimation appears to be the same for uniaxial and constant-width drawing.

It is interesting to consider the evolution of λ^S during drawing. A striking feature of experimental stress–strain curves (*Figures 1* and *2*) is that when the true stress exceeds a value in the region of 10 MPa, all curves show approximately equal rates of strain-stiffening, showing that the increase in λ^S has been arrested. This is readily explained in terms of the orientation-induced crystallization that is known to occur in PET at these temperatures and at strains in the range 1–3[9]. By increasing connectivity of the entangled network, crystallization is expected to increase the viscosity associated with entanglement slippage as shown by Buckley and Salem[10]. Hence (at given stress and constant total strain-rate) it increases the rate of orientation and crystallization, which in turn further increases the viscosity. It is thus an auto-catalytic process, leading rapidly to a lightly-crystallized oriented elastic network with an additional viscous stretch λ^S locked into it. The constitutive model employed here does not introduce such complexity, but results from recent work at Oxford suggested how this may be done[16].

CONCLUSIONS

We have shown that hot-drawing of PET under biaxial stress conforms, within defined limits, to a three-dimensional constitutive model with both glassy and rubbery features. Yield and subsequent flow are consistent with non-Newtonian viscous flow, where the stress-dependence of the viscosity is expressible in terms of the mean stress and octahedral shear stress via Eyring's model of thermal activation. The shear activation volume is so large, however (50 monomer units), that the rate-limiting step must be a highly co-operative event involving many hundreds of atoms. The fact that there is also a small but finite pressure activation volume indicates that this flow event is accompanied by local dilation.

The rubber–elastic contribution to stress can be quantified from the small rubbery plateau visible in isometric stress–temperature plots, and in this way the

rubber-like stress–strain curve constructed. When fitted to the Edwards–Vilgis theory of rubber elasticity, it shows that in PET in the rubbery plateau region the entanglements have no freedom to slide, and so they behave as crosslinks in a thermoset polymer. The length of chain between entanglements is 17 monomer units, according to the present data. Expressed differently: there is one entanglement in a volume of $6\,nm^3$.

Where the current constitutive model deviates from the observed response of PET, it is because of known aspects of behaviour ignored in the version of the model used here. A distribution of relaxation times is required for correctly reproducing the dispersion of viscoelastic response in the time domain, and viscous flow associated with entanglement slippage needs to be introduced to provide the deferral of strain-stiffening observed with increasing temperature above the glass transition. Both features have been discussed elsewhere[16,28]. There is, however, the unresolved question of why measurements of drawing, such as those reported here, imply a degree of flexibility for the PET chain (only 3.2 bonds per freely-orienting unit) that is unrealistically high compared to what is known from other information.

ACKNOWLEDGEMENTS

The authors are indebted to the UK Science and Engineering Research Council for financial support under Co-operative Research Grant E/57349 with ICI Films. They are also grateful for laboratory facilities provided at the Department of Mechanical Engineering, University of Manchester Institute of Science and Technology (UMIST) where the work commenced prior to moving to Oxford, and to Mr C. Hayward (UMIST) and Mr N. Warland (Oxford) for their skilled technical assistance.

REFERENCES

1 Buckley, C. P. and Jones, D. C. *Polymer* 1995, **36**, 3301
2 Ward, I. M. *Polym. Eng. Sci.* 1984, **24**, 724
3 Haward, R. N. and Thackray, G. *Proc. R. Soc.* 1968, **A302**, 453
4 Boyce, M. C. and Arruda, E. M. *Polym. Eng. Sci.* 1990, **30**, 1288
5 Pinnock, P. R. and Ward, I. M. *Trans. Faraday Soc.* 1966, **62**, 1308
6 Rietsch, F., Duckett, R. A. and Ward, I. M. *Polymer* 1979, **20**, 1133
7 Long, S. D. and Ward, I. M. *J. Appl. Polym. Sci.* 1991, **42**, 1921
8 Gordon, D. H., Duckett, R. A. and Ward, I. M. *Polymer* 1994, **35**, 2554
9 Salem, D. R. *Polymer* 1992, **33**, 3182
10 Buckley, C. P. and Salem, D. R. *Polymer* 1987, **28**, 69
11 Jones, D. C. PhD Thesis, Univ. of Manchester, 1993
12 Buckley, C. P. and Sikorski, M. E. *J. Text. Inst.* 1991, **82**, 25
13 Adams, A. M. DPhil Thesis, Univ. of Oxford, 1995
14 Halsey, G., White, H. J. and Eyring, H. *Text. Res. J.* 1945, **15**, 295
15 Edwards, S. F. and Vilgis, Th. *Polymer* 1986, **27**, 483
16 Adams, A. M., Buckley, C. P. and Jones, D. P. Polymer Processing Society, European Regional Meeting, Strasbourg, 1994
17 Kolb, H. J. and Izard, E. F. *J. Appl. Phys.* 1949, **20**, 564
18 Murayama, T., Dumbleton, J. H. and Williams, M. L. *J. Polymer Sci. A-2* 1968, **6**, 1968
19 Vallat, M.-F., Plazek, D. J. and Bhushan, B. *J. Polym. Sci. Polym. Phys. Edn* 1988, **26**, 555
20 Ward, I. M. *Polymer* 1964, **5**, 59
21 Illers, K. H. and Breuer, H. *J. Colloid Sci.* 1963, **18**, 1
22 Argon, A. S. and Bessonov, M. I. *Phil. Mag.* 1977, **35**, 917
23 Mott, P. H., Argon, A. S. and Suter, U. W. *Phil. Mag. A* 1993, **67**, 931
24 Hutnik, M., Argon, A. S. and Suter, U. W. *Macromolecules* 1993, **26**, 1097
25 Wu, S. *J. Polym. Sci; Part B: Polym. Phys.* 1989, **27**, 723
26 Lorentz, G. and Tassin, J. F. *Polymer* 1994, **35**, 3200
27 Flory, P. J. 'The Statistical Mechanics of Chain Molecules', Wiley, New York, 1969
28 Babaiikochekseraii, S. and Buckley, C. P. 8th Int. Conf. on Deformation, Yield and Fracture of Polymers, Plastics and Rubber Institute, Cambridge (UK), 1991
29 Hasan, O. A. and Boyce, M. C. *Polym. Eng. Sci.* 1995, **35**, 331

APPENDIX

Numerical implementation of the constitutive model

A simple, robust and accurate scheme for approximate integration of equation (2) was achieved as follows. The approximation was made that Hencky strains and the viscosity μ varied linearly through the time-step. Thus, using a prime to indicate values applying to the previous time-step, and Δ to indicate time-step increments, we obtain within the time-step: $t = t' + u\Delta t$, where u is a dimensionless time ($0 \leqslant u \leqslant 1$). Equation (2) can then be expressed in terms of u:

$$\frac{ds_i^b}{du} + \left(\frac{\Delta t}{\tau'}\right)\frac{s_i^b}{1+u\delta} = 2G^b\Delta e_i \quad (0 \leqslant u \leqslant 1) \qquad \text{(A1)}$$

where δ is the fractional increase in μ through the time-step: $\Delta\mu/\mu'$. Analytical integration of equation (A1) through the time-step ($u = 0$ to $u = 1$) then yields the increments in deviatoric stresses, which may be written in terms of a tangent shear modulus G^t and history term h as follows

$$\Delta s_i^b = 2G^t\Delta e_i - hs_i^{b'} \qquad \text{(A2)}$$

where

$$G^t = G^b\left(\frac{1+\delta-(1+\delta)^{-\gamma}}{1+\frac{\tau'\delta}{\Delta t}}\right)\frac{\tau'}{\Delta t} \qquad \text{(A3)}$$

$$h = 1-(1+\delta)^{-\gamma}, \qquad \gamma = \frac{\Delta t}{\tau'} \qquad \text{(A4)}$$